Conversion dependent morphology predictions for composite emulsion polymers: 1. Synthetic latices

Catherine L. Winzor and Donald C. Sundberg*
Polymer Research Group, Department of Chemical Engineering, University of New Hampshire, Durham, NH 03824, USA
(Received 16 November 1990; accepted 1 August 1991)

Phase structure develops within composite latex particles during the polymerization process and is potentially dependent upon both the latex recipe and the polymerization process characteristics. An equilibrium thermodynamic approach is presented to predict the particle morphology as a function of the extent of conversion of a seed latex polymerization reaction. The discussion highlights the role of the monomer as it influences the phase compositions and interfacial tensions throughout the polymerization. It is found that a number of different particle morphologies possess nearly the same total interfacial energy throughout a significant portion of the polymerization reaction and that it is quite likely that occluded structures will form in addition to the more fully phase-separated structures, such as core–shell and hemispheres. Detailed methods to predict the probabilities of forming a variety of different morphologies are presented.

(Keywords: latex; particle morphology; polymerization; interfacial tensions)

INTRODUCTION

Structured latex particles are an extremely important class of materials which find use in coatings, adhesives, impact resistant plastics and other varied applications. The control of the particle morphology is critical to achieving desirable physical properties and is a subject of increasing frequency of discussion in the literature. A wide variety of particle morphologies has been reported in the literature over the past decade, including core–shell[1–5], 'inverted' core–shell[1,6,7], sandwich structures[1], hemispheres[1,8], and 'confetti-like', 'raspberry-like' and 'void' particles[9]. It is also evident from viewing microtomed sections of commercial resins that combinations of these morphologies also exist. However, in spite of the importance of morphology control in latex particles, there have been relatively few reports in the literature which attempt to develop a general understanding of the factors which control the particle structure. Lee[2] presented a very useful qualitative description of a variety of factors controlling particle morphology. Stutman *et al.*[8] reported on the influence of a large number of experimental variables on the observed morphology of poly(butyl acrylate)/polystyrene (PSTY) latex particles. Sundberg and co-workers[10–12] have offered a theoretical framework based upon equilibrium surface thermodynamics in which the role of interfacial tensions was highlighted. As a result of such an analysis, it was clear that the type of surfactant used to achieve colloidal stability could have a dramatic effect upon the final morphology achieved.

There are several types of theoretical analyses that might be attempted in order to predict the particle morphology. These would include the equilibrium analysis noted above[10–12] in which the objective was to predict the morphology only at the end of the process. In such an instance, one does not need to be concerned with the presence of any monomer or solvent within the particle. As a result, however, no information can be gained about the manner in which the particle morphology evolves during the process. The opposite extreme would seem to be to attempt an analysis based upon the potentially interdependent rate processes of polymerization reaction and phase separation. Both rate processes, especially the latter, are rather difficult to describe accurately and such an effort will be left to further work. The purpose of this paper is to present an equilibrium thermodynamic analysis which deals with the influence of monomer (or solvent) on the interfacial properties of the composite particle as a function of the extent of the process. Such an analysis can yield predictions of conversion-dependent morphology in the limit when phase-separation kinetics can keep pace with reaction kinetics.

Since composite latex particles can be produced from either the synthetic route (monomer reaction within a seed latex particle) or the artificial route (physical removal of solvent from two-component, preformed particles), the theoretical morphology analysis should be able to address both processes. *Figure 1* shows the process pathways for each process from which the same overall composite particles might be formed. Although there are many similarities between the analyses along each pathway, there are enough differences to warrant separate discussions. As such, the following analysis applies only to the synthetic latex process; that for the artificial latex process is described in a separate communication.

*To whom correspondence should be addressed

0032-3861/92/183797-14

THERMODYNAMIC CONSIDERATIONS

In a previous paper[11] we showed that the driving force for morphology development was equivalent to the Gibbs free energy change for the process. This was done by considering a hypothetical pathway with the initial state being pure polymer 1 particles suspended in water (and surfactant if present), and a separate, bulk phase of incompatible polymer 2. The final state was considered to be one of four possible two-phase polymer 1–polymer 2 morphologies; core–shell (CSOP), inverse core–shell (CSPO), hemisphere (HS) and individual particles (IP). The equations for the reduced surface energies which were derived for each morphology in the above paper allow the prediction of the final 'equilibrium' morphology; they were not meant to suggest possible pathways of morphology development – only the final morphology.

In this paper we are considering reactive systems, where polymerization takes place in monomer-swollen seed particles leading to phase separation and the formation of two-phase particles. Here it is no longer appropriate for the reference (or initial state) to comprise merely particles of polymer 1 and a bulk phase of polymer 2. The third component, monomer 2, must be introduced. Two alternatives exist for a new reference state: (i) a monomer-swollen polymer 1 particle with a separate bulk phase of polymer 2 or (ii) a polymer 1 particle with separate bulk phases of polymer 2 and monomer 2. While the first alternative is more closely related to experimental conditions, the second is equally as valid and provides a ready comparison with the equations of our earlier paper[11] since the contribution of the reference state to the reduced surface energy equations for alternative morphologies remains the same. This situation is depicted in *Figure 2*.

In a typical batch seeded polymerization, the initial polymer 1 particles are swollen with monomer 2. Once polymerization commences, phase separation of polymer 2 will occur and monomer 2 will partition between the two phases. We now have to consider the influence of monomer in each phase. The presence of monomer will affect the interfacial tensions between the polymer phases and the aqueous phase as well as the polymer–polymer interfacial tension. Additionally, the volumes of each phase will change during polymerization as monomer is consumed and shrinkage occurs.

In the following expressions for the change in free energy for each possible morphology, terms due to enthalpies of mixing, demixing and reaction have been neglected. This is justified since ultimately we are considering the difference in the various ΔG terms for each morphology and such enthalpy terms will cancel. Thus, we need only consider the creation of new interfaces in deriving the free energy change for each morphology. These interfaces are: (polymer 1, monomer 2)/water, (polymer 2, monomer 2)/water and (polymer 1, monomer 2)/(polymer 2, monomer 2), while the only interface for the reference state is polymer 1/water. The interfacial tensions will be influenced by the presence of surfactant and the amount of monomer present. This will be discussed in more detail later.

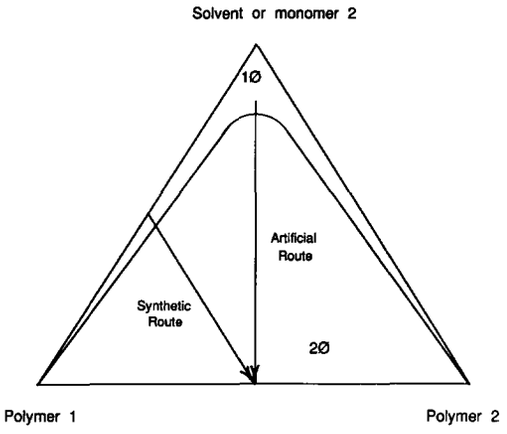

Figure 1 Phase diagram for three-component system showing synthetic (reactive) and artificial processing routes

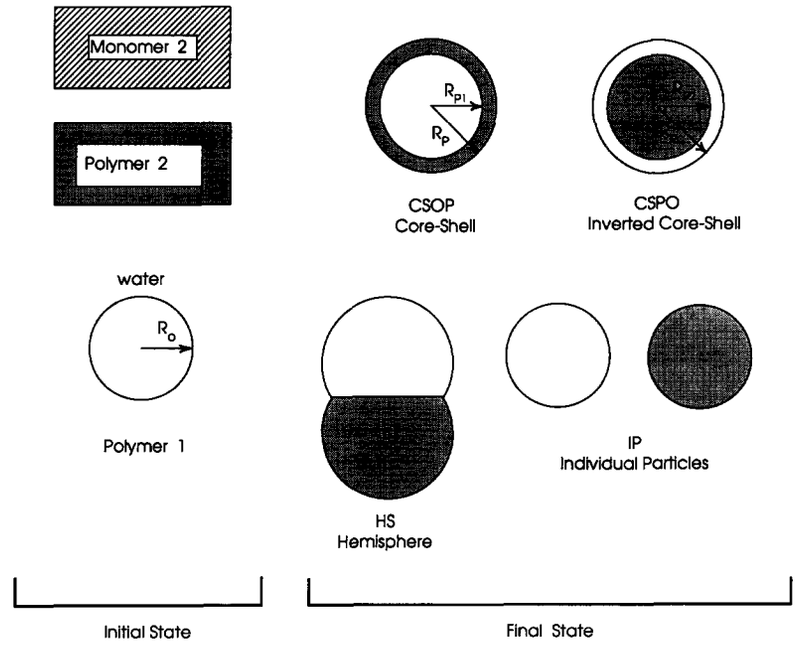

Figure 2 Initial (reference) and final states for morphology development (basic morphologies)

For all of the morphologies represented in *Figure 2*, the change in free energy can be expressed as:

$$\Delta G = \sum_i \gamma_i A_i - \gamma_{P1/W} A'_0 \quad (1)$$

where γ_i is the interfacial tension of the ith interface and A_i is the corresponding interfacial area. Thus $\gamma_{P1/W}$ is the interfacial tension of the original polymer 1 particle suspended in water (and surfactant) and A'_0 is its interfacial area. The $\gamma_{P1/W}A'_0$ term corresponds to the reference energy state. Each different particle morphology differs only in geometry, leading to different expressions for $\sum \gamma_i A_i$. In our earlier paper[11] we obtained expressions for $(\Delta\gamma)$, the reduced free energy change, which was obtained by dividing the expression for ΔG by the reference area:

$$(\Delta\gamma) = \Delta G / A'_0 \quad (2)$$

The equations were derived in terms of the volume fraction of polymer 2 in the particle (ϕ_p). For a polymerizing system, the volume fraction of polymer 2 depends on the densities of the polymers and monomers (ρ_{P1}, ρ_{P2}, ρ_{M2}), the partition coefficients of monomer 2 between the two polymer phases and between the polymer phases and the aqueous phase, and upon the conversion (X) of monomer 2 to polymer 2. In order to predict possible morphology changes during polymerization, it is beneficial to express the reduced free energies as a function of conversion rather than volume fraction.

For the simple case of CSOP morphology shown in *Figure 2*, the free energy change is:

$$\Delta G_{CSOP} = \gamma_{P1M2/P2M2} 4\pi (R_{P1})^2 + \gamma_{P2M2/W} 4\pi (R_P)^2 - \gamma_{P1/W} 4\pi (R'_0)^2 \quad (3)$$

where $\gamma_{P1M2/P2M2}$ is the polymer 1/polymer 2 interfacial tension (in the presence of monomer 2), $\gamma_{P2M2/W}$ is the polymer 2/water interfacial tension (in the presence of monomer 2) and $\gamma_{P1/W}$ is the polymer 1 interfacial tension (in the absence of monomer 2). R_{P1} is the radius of the core (containing polymer 1 swollen with monomer 2), R_P is the particle radius (core + shell) and R'_0 is the radius of the reference particle.

The reduced free energy is:

$$(\Delta\gamma)_{CSOP} = \Delta G_{CSOP}/(4\pi R_0^2) = \gamma_{P1M2/P2M2}(R_{P1}/R_0)^2 + \gamma_{P2M2/W}(R_P/R_0)^2 - \gamma_{P1/W} \quad (4)$$

Thus we need to find expressions for the ratios of the core and shell radii to that of the reference particle. Assuming that any volume change of mixing is negligible, these can be written in terms of volumes, and in turn, the densities (ρ) and masses (w) of polymer 1, polymer 2 and monomer 2, and conversion (X). As such:

$$(R_{P1}/R_0)^2 = \{[(w_{P1}/\rho_{P1}) + (w_{M2P1}/\rho_{M2})]/(w_{P1}/\rho_{P1})\}^{2/3} \quad (5)$$

The amount of monomer 2 in the polymer 1 phase, w_{M2P1}, will be dependent on the conversion level and the partition coefficient of monomer between the two polymer phases and the water. Details of the evaluation of the w_{M2P1}/ρ_{M2} term are given in Appendix 1. The particle interfacial area, $(R_P/R_0)^2$ is given by:

$$(R_P/R_0)^2 = (\{(w_{P1}/\rho_{P1}) + [(1-X)w_{M2}/\rho_{M2}] + (Xw_{M2}/\rho_{P2})\}/(w_{P1}/\rho_{P1}))^{2/3} \quad (6)$$

Combining equations (5) and (6) with equation (4) gives the full expression for the reduced surface energy, $(\Delta\gamma)_{CSOP}$.

For the CSPO particle we have:

$$(\Delta\gamma)_{CSPO} = \gamma_{P1M2/P2M2}(R_{P2}/R_0)^2 + \gamma_{P1M2/W}(R_P/R_0)^2 - \gamma_{P1/W} \quad (7)$$

where R_{P2} is the radius of the polymer 2 core (*Figure 2*). Again an expression for the ratio of the radii of the polymer 2 core and the reference particle must be obtained:

$$(R_{P2}/R_0)^2 = \{[(Xw_{M2}/\rho_{P2}) + (w_{M2P2}/\rho_{M2})]/(w_{P1}/\rho_{P1})\}^{2/3} \quad (8)$$

As in the previous case, the amount of monomer 2 in the polymer 2 phase, w_{M2P2}, will be dependent on the conversion and partition coefficient. Calculation details are given in Appendix 1. Substitution of equations (6) and (8) into equation (7) gives the expression for $(\Delta\gamma)_{CSPO}$.

Although the individual particle morphology is unlikely to be obtained in practice, it can serve as a useful reference point for other morphologies.

$$(\Delta\gamma)_{IP} = \gamma_{P1M2/W}(R_{P1}/R_0)^2 + \gamma_{P2M2/W}(R_{P2}/R_0)^2 - \gamma_{P1/W} \quad (9)$$

Substitution of the expressions for $(R_{PI}/R_0)^2$ and $(R_{P2}/R_0)^2$ [equations (5) and (8)] gives the complete equation.

The mathematical treatment of the HS morphology is much more complex, and only the simplified morphology (SHS) depicted in *Figure 3* will be considered here. This reduces to:

$$\Delta G_{SHS} = \gamma_{P1M2/P2M2}(2\pi R_P h - \pi h^2) + \gamma_{P2M2/W}(2\pi R_P h) + \gamma_{P1M2/W}(4\pi R_P^2 - 2\pi R_P h) - \gamma_{P1/W} 4\pi R_0^2 \quad (10)$$

$$(\Delta\gamma)_{SHS} = 0.5(R_P/R_0)^2\{\gamma_{P1M2/P2M2}(h/R_P)[1-0.5(h/R_P)] + \gamma_{P2M2/W}(h/R_P) + \gamma_{P1M2/W}[2-(h/R_P)]\} - \gamma_{P1/W} \quad (11)$$

While we already have an expression for $(R_P/R_0)^2$ [equation (6)], the relationship between h and R_P is still required. The volume ratio of the polymer 2 phase to the total particle provides such an equation:

$$V_{P2}/V_P = 0.75(h/R_P)^2 - 0.25(h/R_P)^3 \quad (12)$$

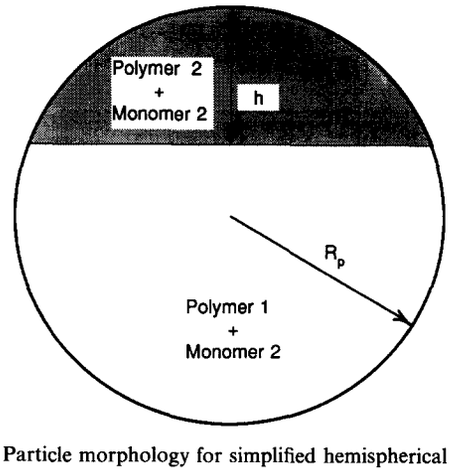

Figure 3 Particle morphology for simplified hemispherical analysis

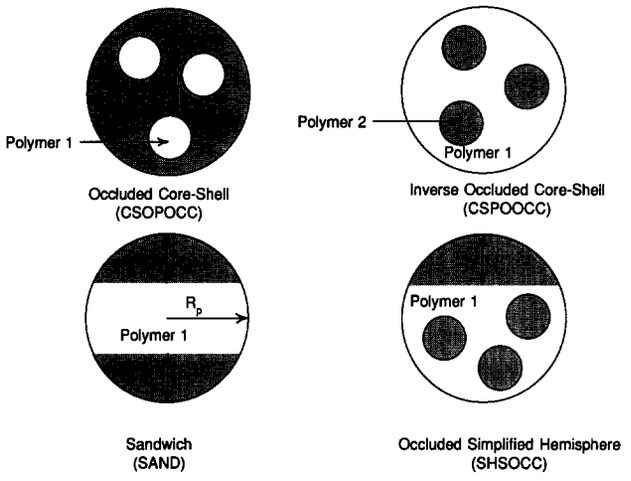

Figure 4 Final states for occluded morphology development

where

$$V_{P2}/V_P = [(Xw_{M2}/\rho_{P2}) + (w_{M2P2}/\rho_{M2})]/\{(w_{P1}/\rho_{P1}) + (Xw_{M2}/\rho_{P2}) + [(1-X)w_{M2}/\rho_{M2}]\} \quad (13)$$

Equations (12) and (13) must be solved to obtain (h/R_P), which then allows the calculation of $(\Delta\gamma)_{SHS}$ via equation (11).

Equations (4), (7), (9) and (11) are similar to those derived in our earlier paper[11]. When $X = 1.0$, i.e. at 100% conversion, we have only polymer 1 and polymer 2, $\gamma_{P1M2/P2M2} = \gamma_{P1/P2}$, $\gamma_{P1M2/W} = \gamma_{P1/W}$ and $\gamma_{P2M2/W} = \gamma_{P2/W}$ and the equations can be reduced to their earlier counterparts.

During polymerization of polymer microparticles swollen with monomer there are two kinetic effects. The first is the kinetics of phase separation, the second, the kinetics of polymerization. It is readily conceived that the latter may override the former; that is, phase separation may not proceed to the equilibrium morphology predicted for a polymer–polymer system, but rather may cease due to the decreased ability of the polymer chains to diffuse within the increasingly more viscous separated phases. In a polymerizing particle it is possible that the resistance due to increasing viscosity will prevent the formation of the simple, completely phase-separated equilibrium morphologies that we have considered so far. In such cases, particles with occlusions or multiple lobes may be favoured, and it is useful to describe their reduced surface energy expressions.

Occluded morphologies

Several occluded morphologies that we will consider are shown in *Figure 4*; these are occluded core–shell (CSOPOCC), occluded inverse core–shell (CSPOOCC), a sandwich structure (SHS with two lobes, SAND) and an occluded hemisphere (SHSOCC).

The reduced free energy changes for CSOPOCC and CSPOOCC structures differ from the unoccluded structures only in the presence of a term $N^{1/3}$, where N is the number of occlusions.

$$(\Delta\gamma)_{CSOPOCC} = \gamma_{P1M2/P2M2}N^{1/3}(R_{P1}/R_0)^2 + \gamma_{P2M2/W}(R_P/R_0)^2 - \gamma_{P1/W} \quad (14)$$

$$(\Delta\gamma)_{CSPOOCC} = \gamma_{P1M2/P2M2}N^{1/3}(R_{P2}/R_0)^2 + \gamma_{P2M2/W}(R_P/R_0)^2 - \gamma_{P1/W} \quad (15)$$

where $(R_{P1}/R_0)^2$, $(R_{P2}/R_0)^2$ and $(R_P/R_0)^2$ are calculated from equations (5), (8) and (6), respectively. Note that N only appears in one term of each equation, that being a reflection of the fact that occlusions can only form in one phase and not the other.

Similarly, the reduced free energy change for a sandwich-like morphology, with two identical lobes, differs by a factor of two from the equations derived for the SHS morphology.

$$(\Delta\gamma)_{SAND} = (R_P/R_0)^2[\gamma_{P1M2/P2M2}(h_S/R_P)(1 - h_S/2R_P) + \gamma_{P2M2/W}(h_S/R_P) + \gamma_{P1M2/W}(1 - h_S/R_P)] - \gamma_{P1/W} \quad (16)$$

where h_S is the height of the sandwich lobe (see *Figure 4*, cf. h for the SHS of *Figure 3*). Analogous to the SHS, a relationship is required for h_S/R_P:

$$V_{P2}/V_P = 1.5(h_S/R_P)^2 - 0.5(h_S/R_P)^3 \quad (17)$$

Equations (13) and (17) are used to solve for h_S/R_P, and then combined with equations (16) to give the reduced surface energy change for the sandwich morphology.

The final morphology that we will consider is that of SHSOCC, with polymer 2 as the lobe (or 'cap') and occlusions of polymer 2 within the polymer 1 phase (*Figure 4*).

$$(\Delta\gamma)_{SHSOCC} = 0.5(R_P/R_0)^2\{\gamma_{P1M2/P2M2}[(h/R_P)(1 - h/2R_P) + 2N(R_N/R_P)^2] + \gamma_{P2M2/W}(h/R_P) + \gamma_{P1M2/W}(2 - h/R_P)\} - \gamma_{P1/W} \quad (18)$$

where N is the number of occlusions and h/R_P is the ratio of the height of the lobe to the particle radius. In order to solve this equation, it is necessary to arbitrarily set the fraction (L) of polymer 2 (and monomer 2) in the HS lobe compared to that in the occlusions. Then we can write an expression for (R_N/R_P) in terms of (h/R_P):

$$(R_N/R_P)^2 = \{[(1 - L)/4LN][3(h/R_P)^2 - (h/R_P)^3]\}^{2/3} \quad (19)$$

The equation relating (h/R_P) to the volume ratio of the polymer 2 phase in the particle can be shown to be:

$$V_{P2}/V_P = (1/L)[0.75(h/R_P)^2 - 0.25(h/R_P)^3] \quad (20)$$

If equation (19) is substituted in equation (18), we have

$$(\Delta\gamma)_{SHSOCC} = 0.5(R_P/R_0)^2[\gamma_{P1M2/P2M2}((h/R_P)(1 - h/2R_P) + 2N^{1/3}\{[(1 - L)/L][0.75(h/R_P)^2 - 0.25(h/R_P)^3]\}^{2/3}) + \gamma_{P2M2/W}(h/R_P) + \gamma_{P1M2/W}(2 - h/R_P)] - \gamma_{P1/W} \quad (21)$$

As was the case for the SHS, equations (13) and (20) must be used to determine (h/R_P) before $(\Delta\gamma)_{SHSOCC}$ can be calculated via equation (21).

The reduced surface energy equations for occluded morphologies contain some arbitrariness in that it is necessary to specify the number of occlusions in order to solve the equations. The larger the number of occlusions, the larger the polymer 1/polymer 2 interfacial area becomes. In the case of the SHSOCC morphology, it is also necessary to specify the fraction of polymer 2 in the HS lobe, the remainder being occluded.

It can be seen that these reduced surface energy equations, derived using the revised reference state, require some additional information compared to the original equations of our earlier paper[11]. First, some knowledge of the phase equilibria, i.e. the partitioning

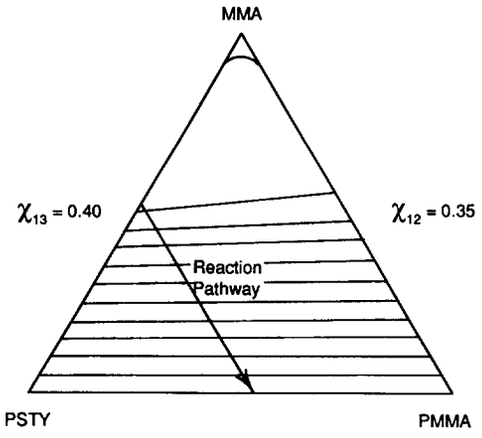

Figure 5 Phase diagram showing tie-lines for polymerizing 50:50 MMA/PSTY particles at 60°C

of monomer between the polymer phases and also between the polymer phases and the aqueous phase, is necessary. Second, and more importantly, the effect of monomer on the polymer/water(surfactant) and polymer/polymer interfacial tensions must be considered. We consider these effects in the next section.

INTERFACIAL PROPERTY CONSIDERATIONS

Distribution of monomer – phase compositions

Before the effects of the presence of monomer on interfacial tensions can be evaluated, it is necessary to determine the amount of monomer in each of the polymer phases, and if the monomer is significantly water-soluble, the amount that partitions into the aqueous phase. Since the calculations are sequential in nature, the distribution of monomer between the polymer particles and the aqueous phase must be considered first.

In calculating the amount of monomer that partitions into the aqueous phase, only two phases are considered; the aqueous phase and a (combined) polymer phase. An estimate of the aqueous partition coefficient (P) can be obtained from the (molal) solubility of the monomer in water (S) using the linear free energy relationship derived by Hansch[13]:

$$\log 1/S = a \log P + b \qquad (22)$$

where a and b are constants that have been derived from studies of many different organic compounds partitioned between iso-octanol and water. Full details of this calculation are given in Appendix 1.

In order to calculate the individual phase compositions, it is necessary to know the nature of the phase diagram. While equations for calculation of the spinodal[14] and binodal[15,16] exist, these calculations (especially the latter) are difficult. If it is assumed that phase separation is complete, then the end points of the tie-lines (at the boundaries of the three-component triangular diagram shown in *Figure 5*) will provide a reasonable estimate of the phase composition. Ideally, the intersection of the binodal with the tie-lines should be used.

Kruse[17] has shown that the equilibrium composition can be given by:

$$\ln(1 - v_3)/(1 - v_2) = v_2 - v_3 + \chi_{12}(v_2)^2 - \chi_{13}(v_3)^2 \qquad (23)$$

where v_2 and v_3 are the volume fractions of polymer 2 and polymer 1, respectively, χ_{12} is the interaction parameter between monomer and polymer 2 and χ_{13} is the interaction parameter between monomer and polymer 1. In this expression, $(1 - v_3)/(1 - v_2)$ is the partition coefficient of the monomer between the two phases. This equation is applicable to high degrees of polymerization and assumes complete phase separation, i.e. the polymer 2 phase contains little (if any) polymer 1 and *vice versa*. At large polymer volume fractions, equation (23) can be simplified to:

$$(1 - v_3)/(1 - v_2) = e^{(\chi_{12} - \chi_{13})} \qquad (24)$$

Comparison of numerical solutions to equations (23) and (24), showed little difference in the calculated tie-line for cases where v_2 or v_3 exceeded 0.25; equation (24) was therefore used in our work.

Thus if χ_{12} and χ_{13} are known (or able to be estimated from the interaction parameters of the polymers with similar solvents) the tie-lines and phase volumes can be computed, and a triangular phase diagram, such as that of *Figure 5*, constructed. The slopes of the tie-lines will depend on the selected values of χ_{12} and χ_{13}, and whether the phase diagram is plotted as volume or weight fractions (the former is preferred). The phase diagram of *Figure 5* was calculated for a 50:50 mixture of methyl methacrylate (MMA)/PSTY polymerized at 60°C using equation (24). In selecting concentration independent values of $\chi_{MMA/PMMA}$ and $\chi_{MMA/PSTY}$ of 0.35 and 0.40, respectively, a range of interaction parameters reported for the polymers in similar solvents was considered[18,19]. Selection of other values for these interaction parameters will, of course, alter the tie-lines and calculated phase compositions.

EFFECT OF MONOMER ON INTERFACIAL TENSIONS

Polymer/polymer interfaces

Measurements of polymer interfacial tensions have shown that there is a significant decrease in interfacial tension when low concentrations of certain additives (such as low molecular weight compounds, block or graft copolymers) are present[20,21]. Thus it might be expected that the presence of large amounts of an additive such as monomer would also affect polymer interfacial tensions. Few actual measurements have been carried out[22–24], but these have shown that the interfacial tension is significantly decreased in the presence of a solvent (often a monomer analogue).

An early attempt at predicting the effect of solvent on such demixed polymer solutions was made by Vrij[25]. More recently, Broseta *et al.*[24] derived the concentration dependence of the interfacial tension for demixed polymer blends in solution using scaling theory and an analogy to the mean field theory of Helfand *et al.*[26–29]. Helfand showed that polymer/polymer interfacial tensions could be predicted using the equation:

$$\gamma_\infty = (kT/a^2)(\chi_{AB}/6)^{0.5} \qquad (25)$$

where a is related to the Kuhn statistical segment length and χ_{AB} is the Flory interaction parameter between the two polymers. Broseta's analogous equations for the solvent-influenced interfacial tension and interfacial

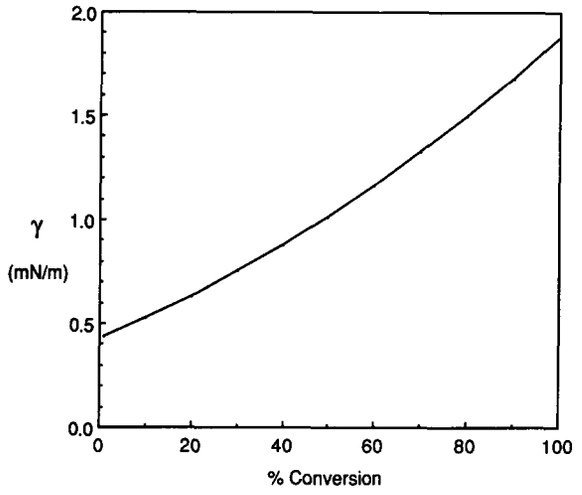

Figure 6 Effect of monomer on polymer/polymer interfacial tensions during polymerization of 50:50 MMA/PSTY particles at 60°C. (—) $\gamma_{PSTY,MMA/PMMA,MMA}$

thickness (D) are:

$$D = \xi/(6u)^{0.5} \quad (26)$$

$$\gamma_\infty = (kT/\xi^2)(u/6)^{0.5} \quad (27)$$

where ξ, the correlation length, and u, the interaction parameter, are concentration dependent. Full details of the calculations of the interfacial tension using equation (27) are given in Appendix 2, together with some comments on the molecular weight and temperature dependences predicted by these equations.

A calculated profile for the monomer-influenced polymer/polymer interfacial tension during polymerization is shown in *Figure 6* for an initially 50:50 MMA/PSTY particle. In these calculations it was assumed that both polymers were of equal molecular weight ($M_n \sim 100\,000$). All of the other parameters are given in Appendix 2. While the interfacial tensions for this example system at low conversion are relatively large, it should be remembered that the particle has a significant polymer concentration before the commencement of polymerization.

Polymer/water interfaces

Just as the presence of low molecular weight additives, such as solvent, has been shown to affect polymer/polymer interfacial tensions, so the presence of solvent (monomer) should be expected to affect the polymer/water interfacial tensions. Experimental measurements of surface tensions of polymer solutions[30,31] have shown two strikingly different concentration profiles, depending on the pure polymer and solvent surface tensions (i.e. whether the polymer surface tension is greater or less than that of the solvent). Prigogine and Marechal[32] developed a simple theory to predict surface tensions of polymer solutions; this was refined by Gaines[30] to predict the concentration dependence in either situation. Siow and Patterson[33] extended the Prigogine–Marechal equations (based on lattice theory) still further to allow the prediction of the effect of solvent on polymer/water interfacial tensions.

Siow and Patterson showed that the solvent-influenced interfacial tension could be calculated via the following equations.

$$[(\gamma - \gamma_1)a]/kT = \ln[(\phi_1^s)/\phi_1] + [(r-1)/r](\phi_2^s - \phi_2) + \chi[l(\phi_2^s)^2 - (l+m)\phi_2^2] \quad (28)$$

$$[(\gamma - \gamma_2)a]/kT = \ln[(\phi_2^s)/\phi_2]^{1/r} + [(r-1)/r](\phi_2^s - \phi_2) + \chi[l(\phi_1^s)^2 - (l+m)\phi_1^2] \quad (29)$$

where ϕ_1 and ϕ_2 are the bulk phase volume fractions of monomer and polymer, ϕ_1^s and ϕ_2^s are the volume fractions of monomer and polymer at the interface, χ is the monomer/polymer interaction parameter, l and m are constants from lattice theory, and a and r are molar volume contributions. Full details of the necessary calculations, including calculation of the volume fractions of the components at the interface, are given in Appendix 2. The magnitude of ϕ_1^s as compared to ϕ_1 will reflect either preferential polymer adsorption or preferential monomer adsorption at the interface. The former will occur when $\gamma_1 > \gamma_2$, i.e. the monomer/water interfacial tension is greater than the polymer/water interfacial tension. Preferential monomer adsorption will occur if $\gamma_2 > \gamma_1$, i.e. the monomer/water interfacial tension is less than that for polymer/water. Both situations are depicted in *Figure 7*, first for STY/PMMA against water containing a natural pectin surfactant Mexpectin XSS100 (MXP XSS100) which shows preferential adsorption of polymer at the interface, and second for MMA/PMMA against water containing sodium lauryl sulphate (SLS), where there is preferential adsorption of monomer at the interface. The interfacial tensions at 0.0 and 1.0 volume fractions of *Figure 7* were measured in this laboratory at room temperature.

Figure 8 shows the calculated interfacial tensions, allowing for the effect of monomer on the polymer/water interfacial tension for a polymerization at 60°C of an initially 50:50 MMA/PSTY particle. It should be noted that the polymer particle already has a 50% polymer loading at the commencement of polymerization, thus even at very low conversions ϕ_2 is nearly 0.5. We therefore see only the almost linear portion of *Figure 7*. The interfacial tension of MMA/water, surfactant used was 3.2 mN m^{-1}, which is significantly lower than the polymer/water, surfactant interfacial tensions of 13.1 and

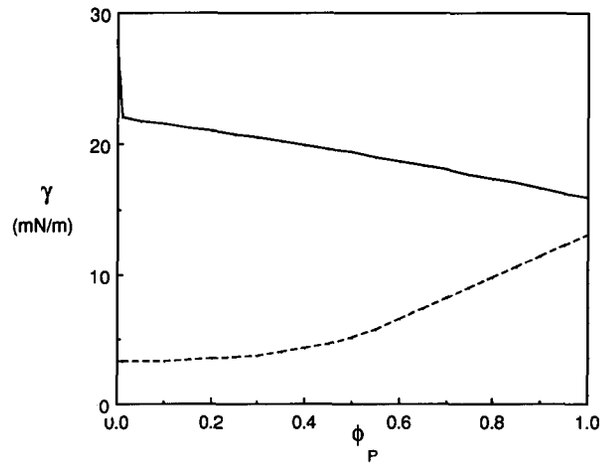

Figure 7 Effect of monomer (volume fraction of polymer, ϕ_P) on polymer/water interfacial tensions. (– – –) Preferential monomer adsorption at interface ($\gamma_{PMMA,MMA/H_2O,MXP}$); (——) preferential polymer adsorption at interface ($\gamma_{PMMA,STY/H_2O,MXP}$)

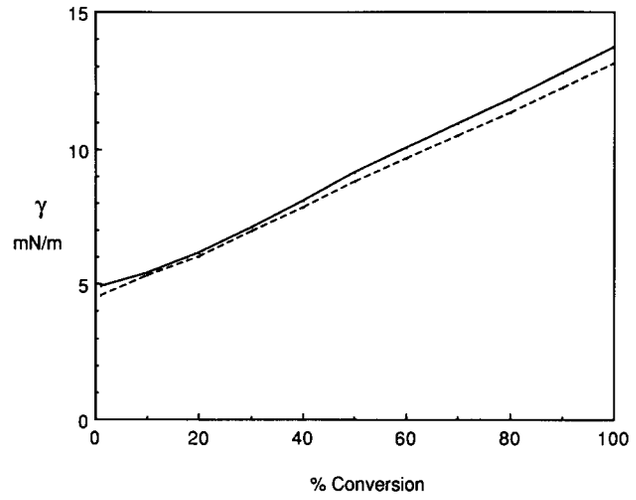

Figure 8 Effect of monomer on polymer/water interfacial tension during polymerization of 50:50 MMA/PSTY particles at 60°C. (——) $\gamma_{PSTY,MMA/H_2O,SLS}$; (– – –) $\gamma_{PMMA,MMA/H_2O,SLS}$

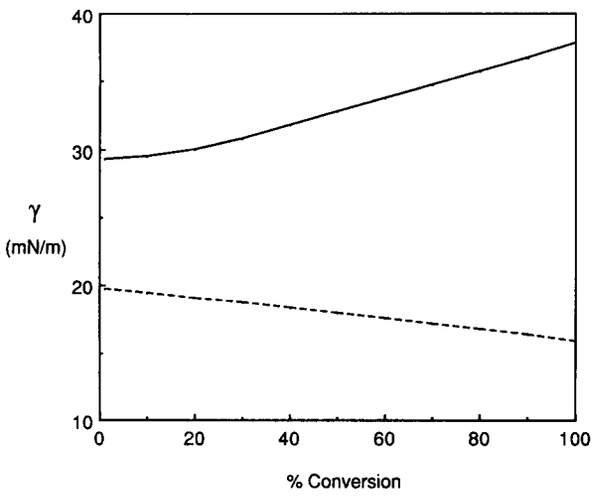

Figure 9 Effect of monomer on polymer/water interfacial tension during polymerization of 50:50 STY/PMMA particles at 60°C (——) $\gamma_{PSTY,STY/H_2O,MXP}$; (– – –) $\gamma_{PMMA,STY/H_2O,MXP}$

13.7 mN m^{-1} for PMMA and PSTY, respectively. These values reflect those reported earlier[11] for polymer/water systems with SLS as surfactant. Thus there is significant adsorption of monomer at the polymer/water interface. The converse situation, of preferential adsorption of polymer at the interface is shown in *Figure 9* for an initially 50:50 STY/PMMA system. Here the following interfacial tensions were used: STY/H_2O = 28 mN m^{-1}, PSTY/H_2O = 37.8 mN m^{-1} and PMMA/H_2O = 15.9 mN m^{-1}, reflecting measured values for systems with MXP XSS100 as surfactant[11]. Again the heavy polymer loading prior to polymerization, means that only a portion of the curve of *Figure 7* is observed.

We now have the means to allow for the estimation of phase compositions (tie-line calculations) and subsequently to predict the various monomer-influenced interfacial tensions as they change during the polymerization reaction. Although the equations which we used require the use of interaction parameters which are sometimes not readily available, the approach we have outlined is fundamental in nature (as opposed to empirical) and thermodynamically sound. We are now in a position to make realistic predictions of composite particle morphology throughout the polymerization process.

PREDICTED MORPHOLOGIES DURING POLYMERIZATION

Once equations for the variation in interfacial areas and interfacial tensions with composition (i.e. conversion of monomer) are available, it is relatively simple to evaluate the various reduced surface energy equations and thus determine the preferred, 'equilibrium' morphology at any point along a reaction pathway. For the purposes of illustration, we will consider a polymerizable seed latex, initially comprising 50:50 MMA/PSTY particles stabilized by SLS. Details of the calculations of the conversion-dependent polymer/water and polymer/polymer interfacial tensions were given in the preceding sections and these profiles are shown in *Figures 8* and *6*, respectively. See Appendix A3 for a sample calculation.

The calculated reduced surface energies ($\Delta\gamma$) for 50:50 MMA/PSTY/SLS particles polymerized at 60°C are shown in *Figure 10* for three of the four basic morphologies, CSOP (with PSTY core), CSPO (PMMA core) and HS. Similar calculations, for a wide variety of polymer/polymer particles, have shown that individual particles are never the preferred morphology, and the $(\Delta\gamma)_{IP}$ curve is therefore omitted from this, and subsequent plots.

Figure 10 shows that at low conversions (<25%), the differences between the ($\Delta\gamma$) curves are very small; <0.5 mN m^{-1}, i.e. ~3% separates the HS and CSPO morphologies. When the energy difference between two morphologies is so small, prediction of one favoured morphology becomes less definite. This is due to limitations on the precision of experimental measurements of interfacial tensions between the polymers (usually extrapolated from measurements on polymer melts[34] or low molecular weight, liquid polymers measured by such techniques as drop-weight-volume[35,36]) and similarly, experimental interfacial tensions for polymers against water/surfactant, e.g. contact angle measurements. The small energy differences at low conversions confer the possibility that more than one morphology may exist

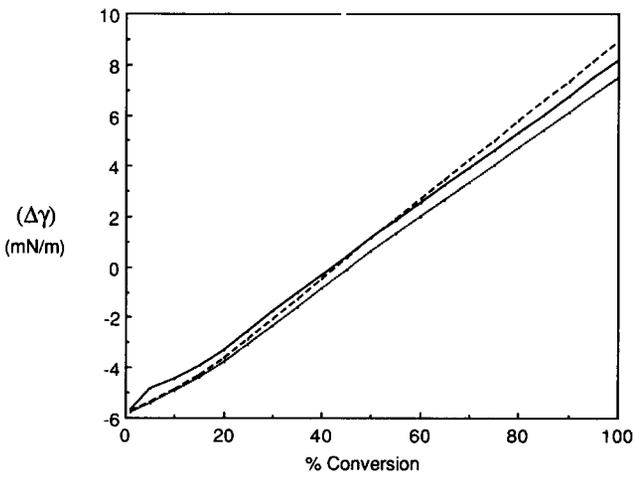

Figure 10 Calculated reduced surface energies for a polymerizing particle (initial composition 50:50 MMA/PSTY, polymerized at 60°C). All interfacial tensions corrected for the effect of monomer ($\gamma_{PSTY,MMA/H_2O,SLS}$, $\gamma_{PMMA,MMA/H_2O,SLS}$ and $\gamma_{PSTY,MMA/PMMA,MMA}$). (——) CSOP; (– – –) CSPO; (· · ·) SHS morphologies

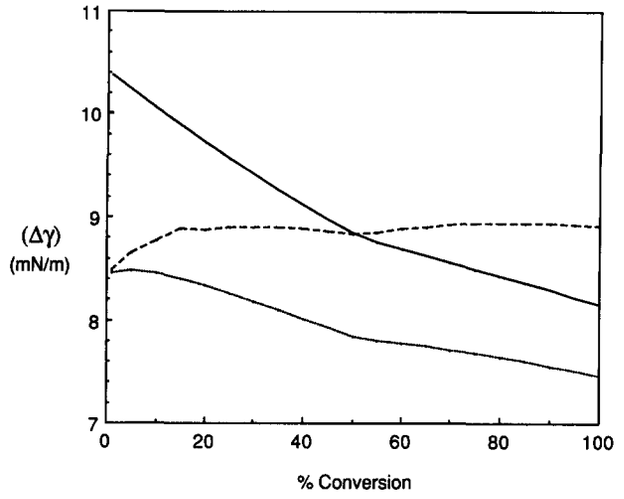

Figure 11 Calculated reduced surface energies for a polymerizing particle (initial composition 50:50 MMA/PSTY, polymerized at 60°C). Effect of monomer on all interfacial tensions ignored ($\gamma_{PSTY/H_2O,SLS}$, $\gamma_{PMMA/H_2O,SLS}$ and $\gamma_{PSTY/PMMA}$). (——) CSOP; (– – –) CSPO; (· · ·) SHS morphologies

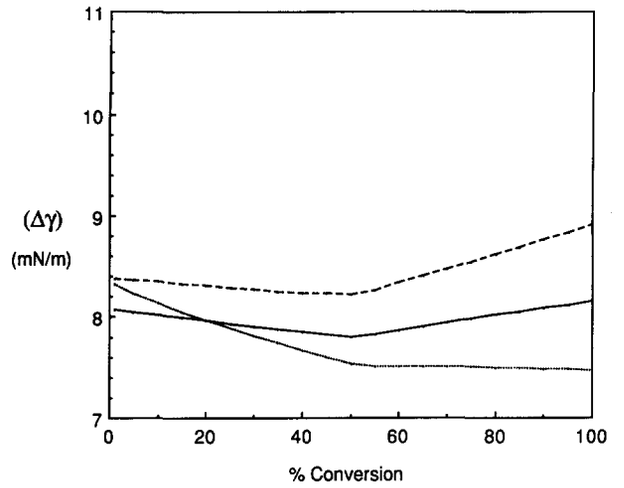

Figure 12 Calculated reduced surface energies for a polymerizing particle (initial composition 50:50 MMA/PSTY, polymerized at 60°C). Polymer/polymer interfacial tension corrected for effect of monomer; effect of monomer on polymer/water interfacial tensions ignored ($\gamma_{PSTY/H_2O,SLS}$, $\gamma_{PMMA/H_2O,SLS}$ and $\gamma_{PSTY,MMA/PMMA,MMA}$). (——) CSOP; (– – –) CSPO; (· · ·) SHS morphologies

among the polymer particles, and that one morphology may become dominant later in the polymerization reaction, provided that the phase separation process is not hindered by the increased viscosity (and decreased rates of diffusion within the particles).

The effects of the contributions of interfacial tensions and interfacial areas can be seen in *Figures 10–13*. In *Figure 10*, the effect of monomer on all of the interfacial tensions ($\gamma_{P1M2/W}$, $\gamma_{P2M2/W}$ and $\gamma_{P1M2/P2M2}$) has been taken into account, as described in the preceding sections. In *Figure 11*, we show what is predicted when the effect of monomer on all of the interfacial tensions is ignored and they are held constant at their 'final', monomer-free, values ($\gamma_{P1/W}$, $\gamma_{P2/W}$ and $\gamma_{P1/P2}$). In this case the only changes with conversion are the interfacial areas. The trends of the ($\Delta\gamma$) curves are rather different from those of *Figure 10*, and there is more separation between them, leading to the expectation that HS morphology would be observed throughout polymerization. In *Figure 12*, we have incorporated the effect of monomer on the polymer/polymer interfacial tension ($\gamma_{P1M2/P1M2}$) but assumed that the polymer/water interfacial tensions are unaffected, and remain at their 'final' values ($\gamma_{P1/W}$, $\gamma_{P2/W}$). Here it would appear that the morphology changes from CSOP to HS during the first 20% of the conversion. Lastly, in *Figure 13*, the polymer/water interfacial tensions have been corrected for the presence of monomer ($\gamma_{P1M2/W}$, $\gamma_{P2M2/W}$) but not the polymer/polymer interfacial tension ($\gamma_{P1/P2}$). This plot has many similarities with *Figure 10*, and reverts to the prediction of HS morphology throughout the reaction.

Comparisons of *Figures 10–13* emphasizes the importance of considering the influences of monomer on *all* of the interfacial tensions, if equilibrium morphologies are to be predicted along the reaction pathway. In particular, neglect of the effect of monomer on the polymer/water interfacial tensions can possibly lead to misleading morphology predictions. Although the effect of monomer on polymer/polymer interfacial tensions is small, it is only when this too is taken into consideration that the full picture, and the closeness of the energies of the different morphologies becomes apparent.

In consulting *Figures 10–13*, it is not the magnitude of the individual reduced surface energy curves that is important in determining the equilibrium morphology, but rather the difference in magnitude between the curves. It is this feature that allows us to neglect terms of enthalpies of mixing, demixing and reaction in the derivation of the reduced surface energy equations, since at any given conversion, these terms will be equal for each morphology and thus cancel when the difference between morphologies is considered.

During polymerization, the viscosity within the polymer particles increases dramatically and complete phase separation may become difficult to achieve within the timeframe of the polymerization. This will likely lead to the existence of occluded morphologies. *Figure 14* shows the calculated ($\Delta\gamma$) curves for CSOP morphology with an increasing number of occlusions in the core. The differences in these curves are due to the increased

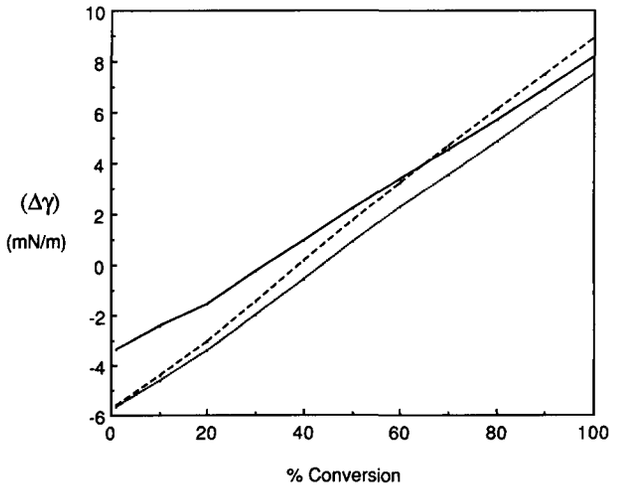

Figure 13 Calculated reduced surface energies for a polymerizing particle (initial composition 50:50 MMA/PSTY, polymerized at 60°C). Polymer/water interfacial tensions corrected for effect of monomer; effect of monomer on polymer/polymer interfacial tension ignored ($\gamma_{PSTY,MMA/H_2O,SLS}$, $\gamma_{PMMA,MMA/H_2O,SLS}$ and $\gamma_{PSTY/PMMA}$). (——) CSOP; (– – –) CSPO; (· · ·) SHS morphologies

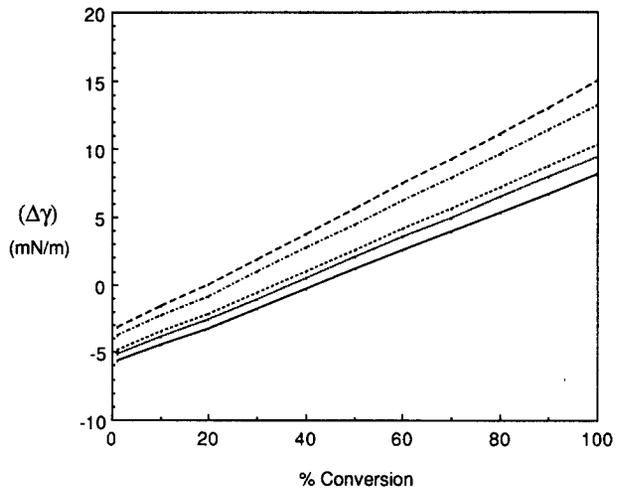

Figure 14 Calculated reduced surface energies (CSOP morphology) for a polymerizing particle (initial composition 50:50 MMA/PSTY, polymerized at 60°C). Effect of increasing the number of occlusions in the particle. (——) CSOP; (···) 5 occlusions; (---) 10 occlusions; (-·-) 50 occlusions; (– – –) 100 occlusions

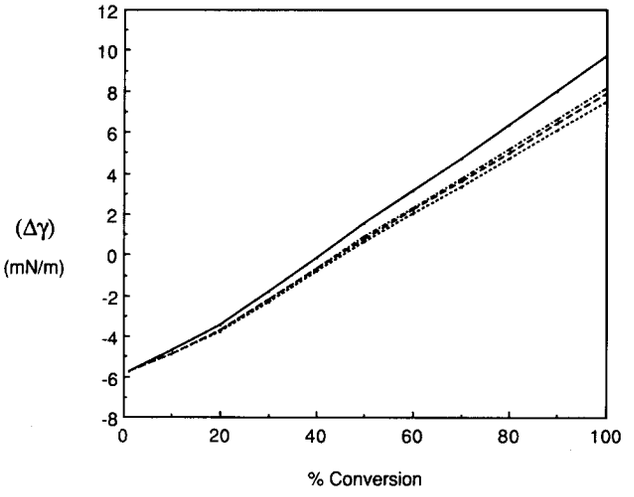

Figure 15 Calculated reduced surface energies for a polymerizing particle (initial composition 50:50 MMA/PSTY, polymerized at 60°C). Possible alternatives to HS morphology (fraction of polymer 2 in lobe: 75%). (---) SHS; (– – –) SAND; (-·-) SHSOCC, 2 occlusions; (——) SHSOCC, 100 occlusions

polymer/polymer interfacial area as the number of occlusions is increased. Recalling equation (14):

$$(\Delta\gamma)_{\text{CSOPOCC}} = \gamma_{\text{P1M2/P2M2}} N^{1/3} (R_{\text{P1}}/R_0)^2 + \gamma_{\text{P2M2/W}} (R_{\text{P}}/R_0)^2 - \gamma_{\text{P1/W}} \quad (30)$$

and that it differs from the $(\Delta\gamma)_{\text{CSOP}}$ equation [equation (4)] only in the presence of the $N^{1/3}$ term, the reduced surface energy will increase with the cube root of the number of occlusions. Similar behaviour will be observed for CSPOOCC morphology, since again, the only difference between the occluded and non-occluded surface energy equations [equations (15) and (7), respectively] is the presence of $N^{1/3}$ in the polymer/polymer interfacial area term. At low conversions, the differences between the calculated $(\Delta\gamma)$ curves for increasing numbers of occlusions are not great. This is due to the small polymer/polymer interfacial tension term (greatly reduced by the presence of large amounts of monomer). This leads to the very real possibility of the formation of occluded morphologies, and polymerization kinetics may at times be expected to preclude the attainment of later, more fully phase-separated equilibrium morphologies.

A variation on occluded structures for HS morphologies is the sandwich-like structure. We have previously shown[12] that multiple lobes of sandwich structures will merge with time if the polymer particle retains a low viscosity. In polymerizing particles the diffusion resistance provided by the increased viscosity may be too great for coalescence of the lobes to occur. In deriving the reduced surface energy equations for this morphology, two equal lobes were assumed. *Figure 15* shows $(\Delta\gamma)$ curves for some possible SHSOCC morphologies. At all times during polymerization, the separation between the sandwich and SHS morphologies is very small. The curve calculated for a HS with two occlusions is also indistinguishable at low conversions. Increasing the number of occlusions from 2 to 100 has very little effect until the conversion exceeds 40%.

The calculations for the SHSOCC morphology are somewhat arbitrary, in that it is necessary to set the fraction (L) of polymer 2 forming the lobe, the remainder being present as occlusions in the polymer 1 phase. The effect of varying this fraction is shown in *Figure 16*, and demonstrates the relative contribution of the various polymer interfacial tension and area terms. At low conversions (*Figure 16a*), the polymer/polymer interfacial tension is small due to the high monomer concentration. A 20-fold increase in the number of occlusions (from 5 to 100) has very little effect on the calculated reduced surface energy. As the conversion increases and monomer is consumed (*Figures 16b–d*), the polymer/polymer interfacial tension increases, as does its contribution to the reduced surface energy. Decreasing the amount of polymer present in the lobe increases the interfacial area term for the occlusions causing an increased separation of the surface energy curves as the number of occlusions is increased.

Having seen that at low conversions, the calculated reduced surface energy curves lie very close together

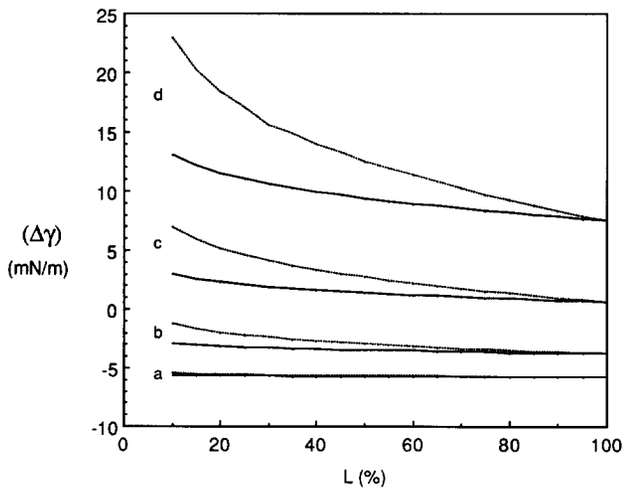

Figure 16 Calculated reduced surface energies (SHSOCC morphology) for a polymerizing particle (initial composition 50:50 MMA/PSTY, polymerized at 60°C). Effects of varying the amount of polymer 2 (PMMA) in lobe and the number of occlusions in the polymer 1 (PSTY) phase. (——) Five occlusions; (····) 100 occlusions: (a) 1% conversion; (b) 20% conversion; (c) 50% conversion; (d) 100% conversion

(even for morphologies with large numbers of occlusions) it becomes apparent that in systems such as the one we have considered, it may be unlikely that just a single morphology would be observed during the polymerization of the polymer particle. At low conversions, the closeness of the curves indicates the possible coexistence of a variety of occluded morphologies, as well as the SHS that is of lowest energy. At high conversions, although the separation of the energy curves has increased, conditions within the particle may inhibit the attainment of the preferred, HS morphology, and occluded morphologies might well be observed.

CONCLUDING REMARKS

In this paper, we have extended our earlier thermodynamic equilibrium approach for the prediction of 'final' equilibrium composite polymer particle morphologies. This allows the prediction of intermediate equilibrium morphologies along the reaction pathway during the polymerization of monomer-swollen seed particles. Evaluation of the reduced surface energy equations requires knowledge of individual phase compositions and the interfacial tensions between the polymer phases and between the polymer phases and the aqueous phase. We have presented some possible methods for calculating these effects and have demonstrated the importance of considering the effect of monomer on all of the interfacial tensions.

As a consequence of this work, it becomes apparent that under reactive processing conditions, the dominance of a single equilibrium morphology may not always be likely. The competition between phase separation and polymerization kinetics can lead to the existence of a range of occluded morphologies due to the small energy differences between the different morphologies during polymerization. These small energy differences combined with the diffusional resistance provided by the high viscosity of the polymerizing phase can possibly prevent coalescence of occlusions to yield fully phase-separated morphologies.

In future papers we will discuss particle morphology development along the artificial processing route, i.e. two incompatible polymers dissolved in a mutual solvent, and present some dynamic studies illustrating the competitive rates of phase separation and polymerization.

ACKNOWLEDGEMENTS

We are grateful for the financial support provided by the donors of the Petroleum Research Fund of the American Chemical Society and for the helpful technical discussions with Nai-Jen Huang.

REFERENCES

1 Cho, I. and Lee, K.-W. *J. Appl. Polym. Sci.* 1985, **30**, 1903
2 Lee, D. I. in 'Emulsion Polymers and Emulsion Polymerization' (Eds D. R. Bassett and A. E. Hamielec), American Chemical Society, Washington, DC, 1981, p. 405
3 Min, T. I., Klein, A., El-Aasser, M. S. and Vanderhoff, J. W. *J. Polym. Sci., Polym. Chem. Edn* 1983, **21**, 2845
4 Hourston, D. J., Satgurunathan, R. and Varma, H. *J. Appl. Polym. Sci.* 1986, **31**, 1955
5 Hourston, D. J., Satgurunathan, R. and Varma, H. *J. Appl. Polym. Sci.* 1987, **33**, 215
6 Muroi, S., Hashimoto, H. and Hosoi, K. *J. Polym. Sci., Polym. Chem. Edn* 1984, **22**, 1365
7 Lee, D. I. and Ishikawa, T. *J. Polym. Sci., Polym. Chem. Edn* 1983, **21**, 147
8 Stutman, D. R., Klein, A., El-Aasser, M. S. and Vanderhoff, J. W. *Ind. Eng. Chem. Prod. Res. Dev.* 1985, **24**, 404
9 Okubo, M., Katsuta, Y. and Matsumoto, T. *J. Polym. Sci., Polym. Lett. Edn* 1982, **20**, 45
10 Berg, J., Sundberg, D. and Kronberg, B. *J. Microencapsulation* 1989, **6**, 327
11 Sundberg, D. C., Cassasa, A. J., Pantazopoulos, J., Muscato, M. R., Kronberg, B. and Berg, J. *J. Appl. Polym. Sci.* 1990, **41**, 1425
12 Muscato, M. R. and Sundberg, D. C. *J. Polym. Sci., Polym. Phys. Edn* 1991, **29**, 1021
13 Hansch, C., Quinlan, J. E. and Lawrence, G. L. *J. Org. Chem.* 1968, **33**, 347
14 Zeman, L. and Patterson, D. *Macromolecules* 1972, **5**, 513
15 Scott, R. L. *J. Chem. Phys.* 1949, **17**, 279
16 Hsu, C. C. and Prausnitz, J. M. *Macromolecules* 1974, **7**, 320
17 Kruse, R. L. in 'Copolymers, Polyblends and Composites' (Ed. N. A. J. Platzer), American Chemical Society, Washington, DC, 1975, p. 141
18 Tseng, T. M., El-Aasser, M. S. and Vanderhoff, J. W. in 'Computer Applications in Applied Polymer Science' (Ed. T. Provder), American Chemical Society, Washington, DC, 1982, p. 197
19 Barton, A. F. M. 'CRC Handbook of Solubility Parameters and Other Cohesion Parameters', CRC Press, Boca Raton, 1983, pp. 254–261
20 Wu, S. 'Polymer Interface and Adhesion', Marcel Dekker, New York, 1982, pp. 72, 122–128
21 Patterson, H. T., Hu, K. T. and Grindstaff, T. H. *J. Polym. Sci.* 1971, **C34**, 31
22 Langhammer, G. and Nester, L. *Makromol. Chem.* 1965, **88**, 179
23 Nose, T. and Tan, T. V. *J. Polym. Sci., Polym. Lett. Edn* 1976, **14**, 705
24 Broseta, D., Leibler, L., Kaddour, L. O. and Strazielle, C. *J. Chem. Phys.* 1987, **87**, 7248
25 Vrij, A. *J. Polym. Sci. A2* 1968, **6**, 1919
26 Helfand, E. and Tagani, Y. *J. Polym. Sci.* 1971, **B9**, 741
27 Helfand, E. and Tagani, Y. *J. Chem. Phys.* 1972, **56**, 3592
28 Helfand, E. and Tagani, Y. *J. Chem. Phys.* 1972, **57**, 1812
29 Helfand, E. and Sapse, A. M. *J. Chem. Phys.* 1975, **62**, 1327
30 Gaines, G. L. *J. Phys. Chem.* 1969, **73**, 3143
31 Gaines, G. L. *J. Polym. Sci. A2* 1969, **7**, 1379
32 Prigogine, I. and Marechal, J. *J. Colloid Sci.* 1952, **7**, 122
33 Siow, K. S. and Patterson, D. *J. Phys. Chem.* 1973, **77**, 356
34 Wu, S. *J. Phys. Chem.* 1970, **74**, 632
35 Lando, J. L. and Oakley, H. T. *J. Colloid Interface Sci.* 1967, **25**, 526
36 Anastasiadis, S., Gancarz, I. and Koberstein, J. T. *Macromolecules* 1988, **21**, 2980
37 Leo, A. J. in 'Biological Correlations – The Hansch Approach' (Ed. W. V. Valkenburg), American Chemical Society, Washington DC, 1970, p. 51
38 Grant, D. J. W. and Higuchi, T. 'Solubility Behavior of Organic Compounds', Wiley Interscience, New York, 1990
39 Kaddour, L. O., Anastagasti, M. S. and Strazielle, C. *Makromol. Chem.* 1987, **188**, 2223
40 Flory, P. J. 'Principles of Polymer Chemistry', Cornell University Press, Ithaca, 1953, pp. 428–430, 515
41 Kurata, M. and Stockmayer, W. H. *Fortschr. Hochpolym. Forsch.* 1963, **3**, 196
42 Russell, T. P., Hjelm, R. P. and Seeger, P. A. *Macromolecules* 1990, **23**, 890
43 Tanaka, T. and Inagaki, H. *Macromolecules* 1979, **12**, 1229
44 Fukuda, T., Nagata, M. and Inagaki, H. *Macromolecules* 1984, **17**, 548
45 Fukuda, T., Nagata, M. and Inagaki, H. *Macromolecules* 1986, **19**, 1411
46 Su, A. C. and Fried, J. R. *Macromolecules* 1986, **19**, 1417
47 Fernandez, M. L., Higgins, J. S., Penfold, J., Ward, R. C., Shackleton, C. and Walsh, D. J. *Polymer* 1988, **29**, 1923
48 Broseta, D., Fredrickson, G. H., Helfand, E. and Leibler, L. *Macromolecules* 1990, **23**, 132
49 Bawn, C. E. H., Freeman, R. F. J. and Kamaliddin, A. R. *Trans. Faraday Soc.* 1950, **46**, 677
50 Gee, G. *J. Chem. Soc.* 1947, 280

APPENDIX 1

Evaluation of amount of monomer in polymer phases

In order to calculate the interfacial areas for each morphology, we have assumed that the volume of mixing term is negligible and summed the volumes of each component. For example, for the 'core' of the CSOP morphology, equation (5) was derived:

$$(R_{P1}/R_0)^2 = \{[(w_{P1}/\rho_{P1}) + (w_{M2P1}/\rho_{M2})]/(w_{P1}/\rho_{P1})\}^{2/3} \quad (A1)$$

The term w_{M2P1}/ρ_{M2} represents the volumetric swelling of the polymer 1 phase by monomer. This term is dependent firstly on the partitioning of monomer between the polymer phases and the aqueous phase (if it is water-soluble) and secondly, the partitioning of monomer between the two polymer phases.

Partitioning into the aqueous phase is considered first, since this reduces the amount of monomer available for distribution between the polymer phases. If we define this aqueous partition coefficient, P, as the ratio of the weight fractions of monomer in the total polymer phase to that in the water phase, namely:

$$P = [w_{M2,P}/(w_{P1} + w_{P2})]/(w_{M2,W}/w_W) \quad (A2)$$

then by rearrangement and use of the conversion level, X, it can be shown that:

$$w_{M2,P} = (1 - X)w_{M2}/\{1 + [w_W/P(w_{P1} + Xw_{M2})]\} \quad (A3)$$

P can be estimated from the aqueous molal solubility of the monomer (S) using Hansch parameters[13,37,38] and the equation

$$\log 1/S = a \log P + b \quad (A3a)$$

In a study of 156 organic compounds, Hansch[13] found that $a = 1.339$ and $b = -0.978$ gave a good fit to all of the data for measured partition coefficients between iso-octanol and water. Using the calculated P the amounts of monomer in the aqueous and (combined) polymer phases can be calculated. Obviously, the amount of monomer in the aqueous phase ($w_{M2,W}$) cannot exceed its solubility; it may therefore be necessary to adjust the calculated value of $w_{M2,P}$, since all of the remaining monomer will swell the polymer particles.

The second step is to calculate the volumes of monomer in each of the polymer phases. If the monomer/polymer interaction parameters (χ_{12} and χ_{13}) are known, the tie-lines of the triangular phase diagram can be calculated using Kruse's approach[17]:

$$(1 - v_3)/(1 - v_2) = e^{(\chi_{12} - \chi_{13})} \quad (A4)$$

where v_3 and v_2 are the volume fractions of monomer in the polymer 1 and polymer 2 phases, respectively. Calculation of w_{M2P1} and w_{M2P2} is then straightforward, and the resulting values can be used directly in the calculation of interfacial areas via equations (5), (6), (8) and (13).

Although the above approach is preferred, it may not always be possible to calculate the phase volumes via the tie-line approach. Then the distribution coefficient, K, must be estimated, or measured experimentally. Here we have defined K as:

$$K = (w_{M2P2}/w_{P2})/(w_{M2P1}/w_{P1}) \quad (A5)$$

This definition of the distribution coefficient is analogous to the polymer/water partition coefficient, defined earlier [equation (A2)], but it differs from Kruse's definition (which is the reciprocal, and incorporates the volume of monomer in each phase). It should be noted that if $\chi_{12} = \chi_{13}$, then the two definitions are equivalent, $K = 1$, and there is equal partitioning of the monomer between the two polymer phases.

Using the above definition of K, we obtain:

$$w_{M2P1} = w_{P1}(1 - X)w_{M2}/(KXw_{M2} + w_{P1}) \quad (A6)$$

$$w_{M2P2} = KXw_{M2}(1 - X)w_{M2}/(KXw_{M2} + w_{P1}) \quad (A7)$$

Therefore, equation (5) becomes:

$$(R_{P1}/R_0)^2 = \{[\rho_{M2}(KXw_{M2} + w_{P1}) + \rho_{P1}(1 - X)w_{M2}]/(\rho_{M2}(KXw_{M2} + w_{P1})]\}^{2/3} \quad (A8)$$

Similarly, equation (6) becomes:

$$(R_P/R_0)^2 = \{[\rho_{M2}\rho_{P2}w_{P1} + \rho_{P2}\rho_{P1}(1 - X)w_{M2} + \rho_{M2}\rho_{P1}Xw_{M2}]/\rho_{M2}\rho_{P2}w_{P1}\}^{2/3} \quad (A9)$$

Equation (8) becomes:

$$(R_{P2}/R_0)^2 = \{\rho_{P1}Xw_{M2}[\rho_{M2}(KXw_{M2} + w_{P1}) + \rho_{P2}K(1 - X)w_{M2}]/\rho_{M2}\rho_{P2}w_{P1}(KXw_{M2} + w_{P1})\}^{2/3} \quad (A10)$$

and equation (13) becomes:

$$V_{P2}/V_P = \{\rho_{P1}w_{M2}X[\rho_{M2}(KXw_{M2} + w_{P1}) + \rho_{P2}K(1 - X)w_{M2}]\}/(KXw_{M2} + w_{P1})[\rho_{M2}\rho_{P2}w_{P1} + \rho_{P1}\rho_{P2}(1 - X)w_{M2} + \rho_{M2}\rho_{P1}Xw_{M2}] \quad (A11)$$

APPENDIX 2

Calculation of monomer-influenced interfacial tensions

Polymer/polymer interfacial tensions: Using scaling theory, Broseta *et al.*[24] derived the concentration dependence of the interfacial tension for demixed polymer blends in solution as follows. In the semidilute region (after demixing or phase separation occurs) excluded volume effects become important. The concentration fluctuations are correlated over large distances (ξ) that scale with concentration:

$$\xi(c) \approx c^{-\nu/(3\nu - 1)} \approx c^{-3/4} \quad (A12)$$

Far from the critical point of demixing, the excluded volume effects are screened out, and A–B interactions between unlike monomers (A and B) become important. Thus the polymer blend, dissolved in a good solvent, can be described as chains of 'blobs' of A or B occupying a correlation volume ξ.

The free energy per blob is:

$$F_0/kT = (x/N_b)\ln x + [(1 - x)/N_b]\ln(1 - x) + ux(1 - x) \quad (A13)$$

where N_b ($= M/c\xi^3$) is the number of blobs per chain and u is the interaction parameter. The interaction parameter also shows a concentration dependence:

$$u(c) = c^{\beta/(3\nu - 1)} \approx c^{0.3} \quad (A14)$$

[β is a universal exponent ($= 0.22$), which is denoted as χ in reference 24.] The free energy expression is analogous to the classical mean field expression for free energy, where u corresponds to the Flory interaction parameter, χ_{AB}, and ξ to the monomer correlation length, a.

Helfand and co-workers[26–29] showed that for chains of infiinite molecular weight, the interfacial thickness and interfacial tension are given by:

$$D = a/(6\chi_{AB})^{0.5} \quad \text{(A15)}$$

$$\gamma_\infty = (kT/a^2)(\chi_{AB}/6)^{0.5} \quad \text{(A16)}$$

Analogously, for demixed polymer blends in solution

$$D = \xi/(6u)^{0.5} \approx c^{-\nu/(3\nu-1)-\beta/2(3\nu-1)} \approx c^{-0.9} \quad \text{(A17)}$$

$$\gamma = (kT/\xi^2)(u/6)^{0.5} \approx c^{2\nu/(3\nu-1)+\beta/2(3\nu-1)} \approx c^{1.65} \quad \text{(A18)}$$

The concentration dependences of u and ξ can be calculated fairly easily. In semi-dilute solutions:

$$u(c) = u_0(c/c_K)^{0.3} \quad \text{(A19)}$$

where c_K is the critical concentration of demixing and $u_0 = 2/N_b = 2c_K\xi_K^3/M$. If c_K, M and the correlation length are known, $u(c)$ can be calculated. The correlation length is also concentration dependent:

$$\xi(c)/R_g = 0.43(c/c^*)^{-3/4} \quad \text{(A20)}$$

where c^* is the overlap concentration:

$$c^* = 3M/4\pi R_g^3 N_{AV} \quad \text{(A21)}$$

Thus if R_g, M and c_K are known, the concentration dependence of the polymer/polymer interfacial tension can be calculated.

For PSTY/PMMA, Kaddour *et al.*[39] have measured c_K in benzene solution:

$$c_K = 227M^{-0.615} \quad \text{(A22)}$$

The average radius of gyration R_g can be estimated from the mean end-to-end distance using the equation[40]

$$R_g = (\langle R^2 \rangle/6)^{0.5} \quad \text{(A23)}$$

Kurata and Stockmayer[41] tabulate the relationship between the mean end-to-end distance and molecular weight ($\langle R^2 \rangle^{0.5}/M^{0.5}$) for many polymers. For PMMA and PSTY, $\langle R^2 \rangle^{0.5}/M^{0.5} = 6.4 \times 10^{-9}$ and 6.7×10^{-9} cm g$^{-1/2}$, respectively. Use of these equations leads to a prediction that the interfacial tension will decrease when the molecular weight is increased. This is contrary to experimental findings[36]. Likewise, the calculated value of γ for a 50:50 polymer blend at 20°C is $\sim$1.1 mN m^{-1}, which is significantly lower than that of 3.0 mN m^{-1} reported by Wu[34].

The temperature dependence of χ (the polymer/polymer interaction parameter) should also be considered. Russell *et al.*[42] have recently reported this dependence measured for poly(styrene-*b*-methyl methacrylate) diblock copolymers:

$$\chi = 0.028 + 3.9/T \quad \text{(A24)}$$

At 60°C, this gives $\chi = 0.039$. (Other workers[43–46] have reported a range of values from 0.009 to 0.03.) This value is significantly larger than the calculated u_0 (0.019), however, Russell found that this larger value of χ gave quite good agreement for the prediction of interfacial thickness, a_I, when compared with experimental measurements at room temperature (a_I = 5 nm) reported by Fernandez *et al.*[47].

Using Russell's temperature dependence of χ in Helfand's equation for interfacial tension [equation (A16)] leads to the result that the interfacial tension is predicted to increase with increasing temperature, which is in conflict with many reported measurements of the variation of interfacial tension with temperature[20,34,36]. In noting this discrepancy, Anastasiadis *et al.*[36], attributed it to two possible causes: (i) that Helfand's equation is derived for infinite molecular weight, and (ii) that the temperature dependence of χ derived from measurements on block copolymers may not be applicable to homopolymer/homopolymer blends. Anastasiadis *et al.* back-calculated χ from their experimental data to derive the necessary temperature dependence. If this is done using Wu's results[34] for the temperature dependence of interfacial tension for PSTY/PMMA, the derived relationship is:

$$\chi = -0.184 + 88.0/T \quad \text{(A25)}$$

which is significantly different from that of Russell[42] obtained for a block copolymer.

In order to obtain the correct molecular weight dependence for interfacial tensions of polymers of equal molecular weight, Broseta *et al.*[24] introduced two additional terms.

$$\gamma = \gamma_\infty(1 - \Delta_1 - u\Delta_2) \quad \text{(A26)}$$

where γ_∞ is the previously calculated interfacial tension, $\Delta_1 = \pi^2/6\text{w}$ and $\Delta_2 \approx 1.67$. The term w is the incompatibility ($\text{w} = \chi N$, where N is the degree of polymerization). The critical point of demixing occurs when $\text{w}_K = 2$. In a later paper[48], where the effect of increasing the molecular weight of only one component was considered, this equation was modified to:

$$\gamma = \gamma_\infty[1 - (\pi^2/6)(1/\text{w}_n) + \ldots] \quad \text{(A27)}$$

Higher terms were regarded as insignificant. Thus one final adjustment needs to be made to the calculated interfacial tension to correct for molecular weight effects. Equation (A26) is used if both polymer components are of equal molecular weight; equation (A27) is used where the molecular weights are unequal.

Polymer/water interfacial tensions. A simple theory for the prediction of solvent-influenced interfacial tensions from the polymer/water and solvent/water interfacial tensions was developed by Siow and Patterson[33], extending equations derived by Prigogine and Marechal[32] for the effect of solvent on surface tensions.

The equation to be solved is:

$$\ln[(\phi_2^s/\phi_2)^{1/r}/(\phi_1^s/\phi_1)] = [(\gamma_1 - \gamma_2)a]/kT + \chi(l+m)(\phi_1^2 - \phi_2^2) - l\chi[(\phi_1^s)^2 - (\phi_2^s)^2] \quad \text{(A28)}$$

which is the correct version of Patterson's equation (3). In this equation, ϕ_i is the volume fraction of component i, ϕ_i^s is the volume fraction of component i in the surface (interface) phase, l and m are constants (from lattice theory), a is a molar volume term for the solvent, r is the ratio of the molar volumes of the polymer and solvent and χ is the polymer/solvent interaction parameter.

This equation can be rearranged and solved for ϕ_1^s using numerical methods (such as the secant method):

$$\phi_1^s - \phi_1[(1-\phi_1^s)/(1-\phi_1)]^{1/r}\exp[(\gamma_2 - \gamma_1)a/kT] + \chi(l+m)(1-2\phi_1) + \chi l(2\phi_1^s - 1) = 0 \quad \text{(A29)}$$

The monomer-influenced interfacial tension can then be calculated using equations (A30) or (A31). The ϕ_1^s term will reflect either preferential monomer or polymer

adsorption at the interface.

$$[(\gamma - \gamma_1)a]/kT = \ln(\phi_1^s/\phi_1) + [(r-1)/r](\phi_2^s - \phi_2) + \chi[l(\phi_2^s)^2 - (l+m)\phi_2^2] \quad \text{(A30)}$$

$$[(\gamma - \gamma_2)a]/kT = \ln[\phi_2^s/\phi_2]^{1/r} + [(r-1)/r](\phi_2^s - \phi_2) + \chi[l(\phi_1^s)^2 - (l+m)\phi_1^2] \quad \text{(A31)}$$

where γ_1 is the monomer/water interfacial tension and γ_2 is the polymer/water interfacial tension.

Although there is a molecular weight dependence inherent in r, the influence of the polymer molecular weight on the interfacial tension is quite small. In making these calculations, we have assumed that (i) γ_2 does not vary with molecular weight – this has been shown[20] to be valid for surface tensions if the molecular weight is $> \sim 3000$ and (ii) that χ_{12} (and χ_{13}) does not vary with concentration – this is a far more dubious assumption, especially since we have taken into consideration a concentration dependence for χ_{23} in the treatment of polymer/polymer interfaces. Flory[40] notes that in many cases where either the polymer or the solvent possesses a dipole, χ_{12} varies throughout the concentration range. The trend is solvent-dependent; for PSTY/toluene χ_{12} decreases with increasing polymer concentration, in 2-butanone χ_{12} decreases[49], while in other systems, e.g. rubber in benzene, χ_{12} remains constant[50]. We have elected to assume that χ_{12} does not vary with concentration in our calculations.

APPENDIX 3

Sample calculations

This section describes the series of calculations necessary for the prediction of particle morphology for polymerizing composite particles, namely initially 50:50 MMA/PSTY particles suspended in water containing SLS and polymerized at 60°C to 10% conversion. The appropriate particle composition at 10% conversion is shown in *Table A1*.

Table A1 Assumed composition of synthetic polymer particles (in parts) at 10% conversion

MMA	0.45
PMMA	0.05
PSTY	0.50
Initiator	0.01
Water	3.0
SLS	0.015

Initially, the composition of each phase must be calculated. Methyl methacrylate is somewhat water-soluble ($\sim$1 wt%). Using Hansch parameters, and equation (A3a) as discussed in Appendix 1, the aqueous partition coefficient, P, is calculated to be 30.0. Calculation of the amount of monomer in the polymer ($w_{M2,P}$) and aqueous ($w_{M2,W}$) phases via equation (A3) using this value of P, leads to the result that the amount of monomer available to partition into the aqueous phase would exceed its solubility; therefore $w_{M2,W}$ is set equal to the solubility of MMA in water (0.03 parts in 3.0 parts water).

Once the total amount of monomer available to swell the polymer phases is known, the amount in each phase must be ascertained. Taking the polymer/solvent interaction parameters to be 0.40 and 0.35 for PSTY/MMA and PMMA/MMA, respectively, Kruse's equation [equation (A4) in Appendix 1] can be solved numerically to give the volume fractions of PSTY ($v_3 = 0.541$) and PMMA ($v_2 = 0.517$) in their respective phases at 10% conversion.

Calculation of the monomer-influenced interfacial tension requires knowledge of the molecular weights of the two polymers and the polymer/polymer interaction parameter. Using equations (A19)–(A23) and the parameters of *Table A2*, $u(c)$ and $\xi(c)$ can be calculated. However, the value of u_0 so calculated, gives $\chi = 0.0187$ (u calculated for the pure blend), which is somewhat lower than that predicted at 60°C from the temperature dependence [equation (A24)] of Russell *et al.*[42]. In order to obtain $\chi = 0.04$ (consistent with the experimental measurements of Russell) a revised u_0 ($= 0.0234$) was used. At 10% conversion, the polymer concentration (strictly, polymer density) is 0.56 g cm^{-3}. Thus, $u(0.56) = 0.032$ [equation (A19)], $\xi(0.56) = 7.26 \times 10^{-8}$ cm [equation (A20)] and $\gamma_\infty(0.56) = 0.640$ mN m^{-1} [equation (A18)]. Finally a molecular weight correction is made [equation (A26)]. The incompatibility $w = 40$ ($= \chi N$, the product of the polymer/polymer interaction parameter and the degree of polymerization), leading to $\gamma(0.56) = 0.546$ mN m^{-1}.

Calculation of the polymer/water interfacial tensions requires the solution of equation (A29) to obtain ϕ_1^s (the volume fraction of monomer at the interface). This can be done using numerical techniques (we used the secant method). *Table A3* shows the parameters used to solve equations (A29) and (A30) for the PMMA,MMA/water and PSTY,MMA/water interfaces. At 10% conversion, the volume fractions of monomer in the PMMA and PSTY phases are 0.483 and 0.459, respectively;

Table A2 Parameters used in the calculation of monomer-influenced polymer/polymer interfacial tension for 50:50 composite PMMA/PSTY particles polymerized to 10% conversion at 60°C

	PSTY	PMMA	Composite	Equation
M_n	100000	100000	100000	
$\langle R^2\rangle^{1/2}/M^{1/2}$ (cm g$^{-1/2}$)[a]	6.7×10^{-9}	6.4×10^{-9}		
R_g (cm)	8.65×10^{-7}	8.26×10^{-7}	8.46×10^{-7}	(A23)
c_K (g cm^{-3})			0.191	(A22)
c^* (g cm^{-3})			0.0658	(A21)
ξ_K (cm)			1.701×10^{-7}	(A20)
u_0			0.0108	
c(blend) (g cm^{-3})			1.116	
u(blend)			0.0187	

[a] Ref. 42

Table A3 Parameters used in the calculation of the monomer-influenced polymer/water interfacial tensions for composite particles at 10% conversion

	PMMA/MMA	PSTY/MMA
l^a	0.5	0.5
m^a	0.25	0.25
T (°C)	60	60
χ	0.35	0.40
a	3.14×10^{-15}	3.14×10^{-15}
r	789.9	895.2
ϕ_1	0.483	0.459
ϕ_1^s	1.00	1.00
γ_1 (mN m^{-1})^b	3.2	3.2
γ_2 (mN m^{-1})^c	13.1	13.7
γ (mN m^{-1})	5.3	5.4

[a]Ref. 14
[b]Measured in this laboratory
[c]Ref. 11

the corresponding calculated interfacial tensions are $\gamma_{PMMA,MMA/H_2O} = 5.3$ mN m^{-1} and $\gamma_{PSTY,MMA/H_2O} = 5.4$ mN m^{-1}.

The final step is to calculate the interfacial areas for the different morphologies. Restricting ourselves to the basic morphologies (CSOP, CSPO and SHS) $(R_{P1}/R_0)^2 = 1.51$ [equation (5)], $(R_{P2}/R_0)^2 = 0.31$ [equation (8)] and $(R_P/R_0)^2 = 1.60$ [equation (6)], while $V_{P2}/V_P = 0.085$ giving $h/R_P = 0.36$ [equations (12) and (13)].

Combining all of this information, the reduced surface energy for each morphology can be calculated at 10% conversion [via equations (4), (7) and (10)] giving $(\Delta\gamma)_{CSOP} = -4.45$, $(\Delta\gamma)_{CSPO} = -4.86$ and $(\Delta\gamma)_{SHS} = -4.93$. The predicted morphology would be hemispheres, although it should be noted that all of the reduced surface energies are quite close in value.